

# Evidence of thick halo for spatial-dependent propagation model with cosmic-ray anisotropy

Bing-Qiang Qiao,<sup>1</sup> Yu-Hua Yao,<sup>2,\*</sup> Wei Liu,<sup>1</sup> Qiang Yuan,<sup>3,4</sup> Xiao-Jun Bi,<sup>1,5</sup> Hong-Bo Hu,<sup>1,5</sup> and Yi-Qing Guo<sup>1,5,†</sup>

<sup>1</sup>*Key Laboratory of Particle Astrophysics, Institute of High Energy Physics,  
Chinese Academy of Sciences, Beijing 100049, China*

<sup>2</sup>*College of Physics, Chongqing University, No.55 Daxuecheng South Rd., High-tech District, Chongqing 401331, China*

<sup>3</sup>*Key Laboratory of Dark Matter and Space Astronomy,  
Purple Mountain Observatory, Chinese Academy of Sciences, Nanjing 210008, China*

<sup>4</sup>*School of Astronomy and Space Science, University of Science and Technology of China, Hefei 230026, China*

<sup>5</sup>*University of Chinese Academy of Sciences, 19 A Yuquan Rd, Shijingshan District, Beijing 100049, China*  
(Dated: June 3, 2022)

The spatial-dependent propagation (SDP) model with a nearby source works well to reproduce the co-evolving features of both cosmic-ray (CR) nuclei spectra and anisotropy. However, it is well known that the sun is offset from the galactic plane. This will lead to a dominating anisotropy in the perpendicular direction, which is discrepant with observations. Thus, it is necessary to re-initiate further investigation into the effect of the solar offset. In this work, for the first time to the best of our knowledge, the combined studies of the solar offset, nuclei spectra, and anisotropy are performed based on the SDP model. As a result, to reproduce CR spectra and anisotropy, the thickness of the inner halo ( $Z_{\text{IH}}$ ) increases linearly with the displacement of the Sun. Moreover, the PeV anisotropy could estimate the value of the diffusion coefficient, thus breaking the degeneracy of the diffusion coefficient and halo thickness. Therefore, it is a good approach to constrain the halo thickness. However, the anisotropy in the PeV energy region, as a new probe, might also shed new light on constraining the solar offset. It is hoped that the anisotropy at the energies of  $\sim$  TeV to PeV can be finely measured by a LHAASO experiment, leading to a better understanding of the thick halo.

PACS numbers: Valid PACS appear here

## I. INTRODUCTION

In recent years, great progress has been made on the spectral measurement of cosmic rays (CRs) with balloon-borne and space-borne experiments. The fine structure of spectral hardening of nuclei at 200 GV was observed by ATIC-2 [36], CREAM [9], and PAMELA [3]. AMS-02 also confirmed the hardening with unprecedented precision, although the spectral shapes have a slight discrepancy with each other [27]. At higher energies, the DAMPE observation clearly revealed that the proton spectrum further experiences a spectral softening at  $\sim 13.6$  TeV, with the spectral index changing from  $\sim 2.60$  to  $\sim 2.85$  [11]. Hints of such spectral features were also found previously by CREAM [45] and NUCLEON measurements [13]. These observations have stimulated significant concern among theoretical physical scientists. Solutions that have been proposed to explain the spectral features include the contribution from nearby SNRs [41], the re-acceleration mechanism of old SNR sources [19, 42], the combination effects from different group sources [46, 47], and the spatial-dependent propagation (SDP) of CRs [25, 30, 43].

Owing to diffusive propagation of particles in the galactic magnetic field and the distribution of sources in the galaxy, a small degree of anisotropy in the arrival di-

rection of CRs is predicted. The data from studies of ARGO-YBJ [15, 16], EAS-TOP [2, 4], IceCube/IceTop [1], and Tibet-AS $\gamma$  [10] indicate that the TeV–PeV dipole anisotropy is not described by a simple power law and undergoes a rapid phase flip at an energy of 0.1–0.3 PeV [7]. These features suggest that a new component of CRs is required to understand the complicated energy-dependence anisotropy. Some have claimed that these enigmas were caused by the effect of the regulation of local magnetic field and/or nearby sources [7, 32, 35, 38, 39]. Liu et al. [33] considered a common evolving origin of energy spectra and the large-scale anisotropy as an explanation. They claimed that the spectral softening at approximately 10 TeV is due to a nearby source contribution in addition to the background component. The low-energy ( $\lesssim 100$  TeV) anisotropy is dominated by the local source, while the high-energy anisotropy is due to the background. The transition of the low- and high-energy components occurs at approximately 100 TeV, forming a dip in the amplitude and a flip of the phase from a nearly anti-galactic center direction to the galactic center direction.

Although the structures of the spectra and anisotropy could be explained, one critical factor has been ignored in previous works, i.e., the Sun's offset. Usually, the solar system is assumed to be located at the mid-plane of the galactic disk, and the source distribution is symmetric above and below the disk. Yet, it has long been known that the Sun locates slightly above the galactic plane (toward the north galactic pole). The inferred dis-

\* yaoyh@cqu.edu.cn

† guoyq@ihep.ac.cn

tance above the mid-plane is from several to  $\sim 30$  pc [21, 31, 44]. The offset would induce a net vertical flow outward from the galactic plane, which generates a corresponding anisotropy component. This is totally inconsistent with experimental observations. However, the estimated solar offset has a significant spread of values when employing a variety of different methods, although recent analyses have revealed smaller uncertainties. The combined study of nuclei spectra and anisotropy may shed light on this topic. In this work, further investigation aimed at the anisotropy problem is performed.

The rest of this paper is organized as follows. In Section 2, the model is described, and in Section 3 the results of calculation compared with observation are presented. Finally, conclusions are given in Section 4.

## II. MODEL DESCRIPTION

It is generally believed that supernova remnants (SNRs) are the likely sources of galactic CRs. They can accelerate the CRs to very high energy with the expanding diffusive shocks generated during their active period [17, 18, 20]. Before arriving at Earth, those CRs have traveled in the galaxy for  $\sim 10^7$  years after they diffuse away from the acceleration sites [26]. During the journey, the impacts due to fragmentation and radioactive decay in the inter-stellar medium (ISM) result in the production of secondary particles. Meanwhile, the electrons suffer energy loss in the inter-stellar radiation field (ISRF) and magnetic field. This journey can be described by the propagation equation as

$$\begin{aligned} \frac{\partial \psi(\mathbf{r}, \mathbf{p}, t)}{\partial t} &= q(\mathbf{r}, \mathbf{p}, t) + \nabla \cdot (D_{xx} \nabla \psi - V_c \psi) \\ &+ \frac{\partial}{\partial p} p^2 D_{pp} \frac{\partial}{\partial p} \frac{1}{p^2} \psi - \frac{\partial}{\partial p} [\dot{p} \psi - \frac{p}{3} (\nabla \cdot V_c \psi)] \\ &- \frac{\psi}{\tau_f} - \frac{\psi}{\tau_r}, \end{aligned} \quad (1)$$

where  $q(\mathbf{r}, \mathbf{p}, t)$  are the acceleration sources,  $\psi(\mathbf{r}, \mathbf{p}, t)$  is the density of CR particles per unit momentum  $p$  at position  $\mathbf{r}$ ,  $V_c$  is the convection velocity,  $\dot{p} \equiv dp/dt$  is the momentum loss rate, and  $\tau_f$  and  $\tau_r$  are the characteristic timescales for fragmentation and radioactive decay, respectively.  $D_{xx}$  and  $D_{pp}$  are the diffusion coefficients in coordinate and momentum space, respectively. In fact, the processes of convection ( $V_c$ ) are ignored in this work. Then, the value of  $\psi(\mathbf{r}, \mathbf{p}, t)$  is dependent on the  $D_{xx}$ ,  $q(\mathbf{r}, \mathbf{p}, t)$  and position  $\mathbf{r}$ .

### A. Spatial-Dependent Diffusion

Almost locating in the galactic disk, the galactic astrophysical objects would generate large irregularities of the turbulence and affect the properties of particle diffusion. In the SDP model, the diffusion coefficient is assumed to be anti-correlated with the CR source distribution [28, 43]; the diffusive volume is divided into

two regions as inner halo (IH,  $|z| \leq Z_{IH} = \xi Z_H$ ) and outer halo (OH,  $|z| > Z_{IH}$ ).  $Z_H$  is the half-thickness of the diffusive halo, and  $\xi$  is the ratio of the inner halo to the entire halo with a typical value  $\sim 0.1$ . In the IH region, the level of turbulence is expected to be high due to activities of supernova explosions, and hence the diffusion coefficient is relatively small. The OH region contains scarce active sources, and thus particles diffuse much faster. The diffusion coefficient is parameterized as [28, 34]

$$D_{xx}(\mathbf{r}, z, \mathcal{R}) = D_0 F(\mathbf{r}, z) \beta^\eta \left( \frac{\mathcal{R}}{\mathcal{R}_0} \right)^{\delta_0 F(\mathbf{r}, z)}, \quad (2)$$

where

$$F(\mathbf{r}, z) = \begin{cases} g(\mathbf{r}, z) + [1 - g(\mathbf{r}, z)] \left( \frac{z}{Z_{IH}} \right)^\eta, & |z| \leq Z_{IH} \\ 1, & |z| > Z_{IH}, \end{cases} \quad (3)$$

$$g(\mathbf{r}, z) = \frac{N_m}{1 + f(\mathbf{r}, z)}, \quad (4)$$

where  $f(\mathbf{r}, z)$  is the source density distribution. The numerical package DRAGON [23] is used to solve the transport equation. In this work, the diffusion-reacceleration model is adopted. The injection spectrum of background sources is assumed to be a power law of rigidity with a high-energy exponential cutoff, i.e.,  $q(\mathcal{R}) \propto \mathcal{R}^{-\nu} e^{(-\mathcal{R}/\mathcal{R}_c)}$ . The cutoff rigidity of each element could be either  $Z$ - or  $A$ -dependent. The spatial distribution of sources takes the form of the SNR distribution [22],  $f(\mathbf{r}, z) \propto (r/r_\odot)^{1.69} e^{[-3.33(r-r_\odot)/r_\odot]} e^{(-|z|/z_s)}$ , where  $r_\odot = 8.5$  kpc and  $z_s = 0.2$  kpc.

### B. Local Source

The time-dependent propagation of CRs from the local source is obtained using the Green's function method, assuming a spherical geometry with infinite boundary conditions. The solution is

$$\phi(\mathbf{r}, \mathcal{R}, t) = \frac{q_{inj}(\mathcal{R})}{(\sqrt{2\pi}\sigma)^3} \exp\left(-\frac{r^2}{2\sigma^2}\right), \quad (5)$$

where  $q_{inj}(\mathcal{R})\delta(t)\delta(\mathbf{r})$  is the instantaneous injection spectrum of a point source and  $\sigma(\mathcal{R}, t) = \sqrt{2D(\mathcal{R})t}$  is the effective diffusion length within time  $t$ . The diffusion coefficient  $D(\mathcal{R})$  is taken as the value nearby the solar system. The injection spectrum is again parameterized as a cutoff power-law form,  $q_{inj}(\mathcal{R}) = q_0 \mathcal{R}^{-\alpha} e^{(-\mathcal{R}/\mathcal{R}'_c)}$ . The normalization  $q_0$  is determined through fitting to the GCR energy spectra. The direction of the local source is obtained through fitting to the anisotropy data and to other detailed parameters of the source.

### C. Solar Offset

In the literature, several methods have been adopted to measure the solar offset from the galactic plane, which can be roughly classified into two categories: the matter-based ( $H_{II}$ , molecular and methanol masers) and stars-based (various stars, pulsars, optical stars, wolf-Rayet stars, cepheid variables, magnetars, open clusters) methods. Figure 1 presents estimated offset distances summarized in the Table 1 of Ref. [44], from which it can be seen that the solar offset spans a large range, i.e., from 5 pc to  $\sim 30$  pc, although some analyses have small uncertainties. In the following, the effect of solar offset to the anisotropy is considered.

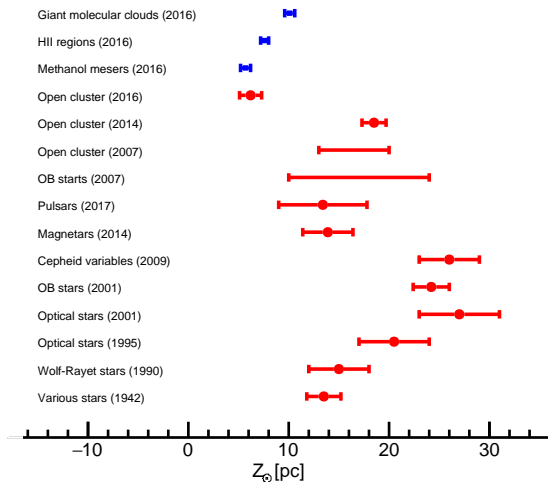


Fig. 1. Displacement of solar offset from the galactic plane summarized in Yao et al. [44]. Red points represent results from different stars-based methods, and the three blue rectangles are results from Bobylev & Bajkova [21] obtained with non-stellar astronomical object methods.

## III. RESULTS

There are several components that might affect CR anisotropy that might remedy the non-conformity of anisotropy because of the above inferred solar offset, namely, the source distribution, inner halo thickness, and outer halo thickness. At the beginning of this work, the effect of each component on the anisotropy was studied by fixing other components and taking solar-offset into account. It was found that, except for the inner halo thickness, the other two components have little influence on the anisotropy. In the following, results of models with different  $Z_{IH}$  are presented.

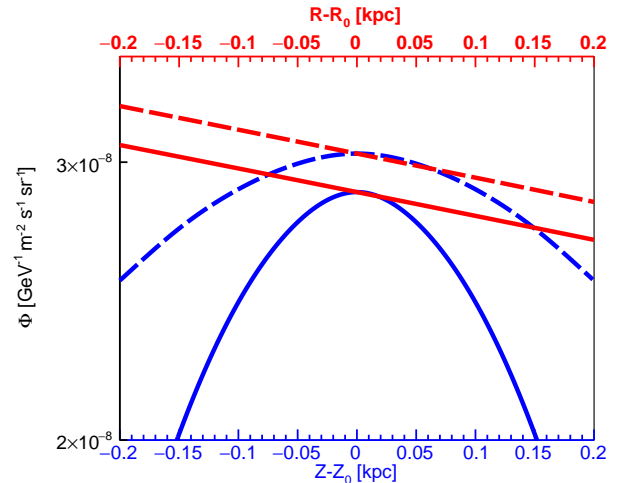


Fig. 2. Schematic of CR fluxes along with distances from  $(R_0, Z_0)$  in vertical (blue) and radial (red) directions. Full (dashed) lines correspond with  $Z_{IH} = 0.5$  (1) and  $(R_0, Z_0) = (8.5, 0)$  kpc, respectively. Dashed lines have been scaled by 0.7 for convenience of comparison.

Table I. Propagation parameters <sup>†</sup>.

$Z_{IH}(\text{kpc})$	$Z_{\odot}(\text{pc})$	$D_0(\times 10^{28} \text{ cm}^2 \text{ s}^{-1})$	$\delta_0$
0.75	5	6.9	0.65
1.0	10	8.75	0.65
1.15	13	9.24	0.69
1.3	16	10.07	0.69
1.45	19	11.05	0.7

<sup>†</sup> $N_m$ ,  $n$ , and  $v_A$  are adopted as 0.39, 3.5, and 6  $\text{km s}^{-1}$ , respectively.

First, the influence of halo thickness on the CR flux density with the Sun's offset is discussed. Then, the propagation parameters under various  $Z_{IH}$  are tuned with B/C, and the CR spectra are obtained with the DRAGON package. Note that the local source mentioned above is also included. Finally, the anisotropy amplitudes and their correlation with the solar vertical displacement from the galactic plane are given.

### A. Effect of Halo Thickness

As shown in Fig. 2, compared with a consistent radial anisotropy (slope of CR flux), the anisotropy in the vertical direction changes significantly with increasing vertical distance from the point  $(R_0, Z_0)$ . Furthermore, the thickness of the halo has strong (little) influence on the vertical (radial) anisotropy. A thicker halo would counteract the vertical CR fluxes caused by the solar offset.

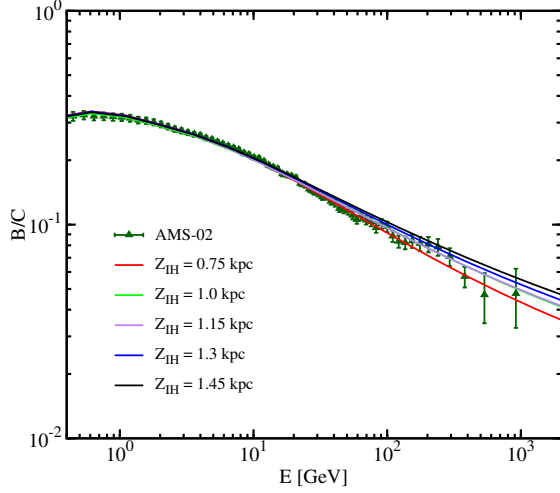


Fig. 3. Model predictions of B/C ratio compared with AMS-02 measurement [5, 6].

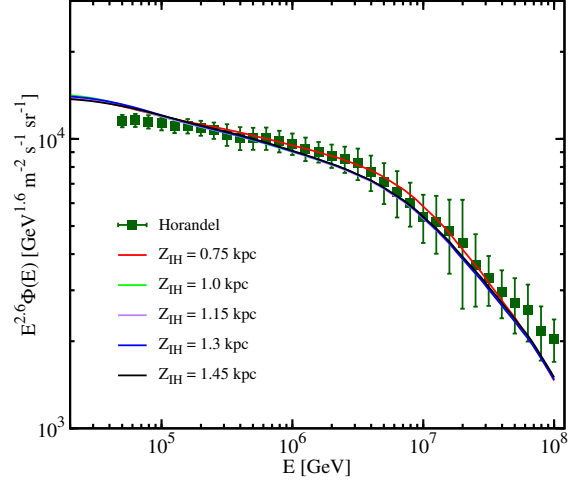


Fig. 5. Model predictions of all-particle spectra at different  $Z_{\text{IH}}$ ; data points are taken from Hörandel [29].

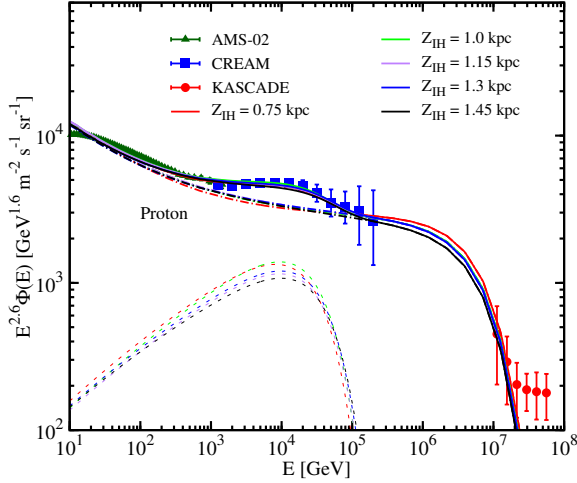


Fig. 4. Model predictions of protons at different  $Z_{\text{IH}}$ , compared with observations from AMS-02 [5, 6], CREAM [9], and KASCADE [12]. Dotted-dashed and dashed lines are fluxes from background and local sources, respectively, and solid lines are their sum. Different colors indicate various  $Z_{\text{IH}}$  scenarios.

### B. B/C and CR Spectra

The transport parameters for the SDP model with different values of  $Z_{\text{IH}}$  are determined by the B/C ratio, as given in Fig. 3. Detailed parameters are presented in Table I. After determination of basic parameters, the propagated spectra of primary CR protons are shown in Fig. 4. It can be seen that the addition of the local source component can simultaneously account for the spectral hardening features at  $\sim 200$  GV and the softening features at  $\sim 10$  TV. Note that there are slight differences

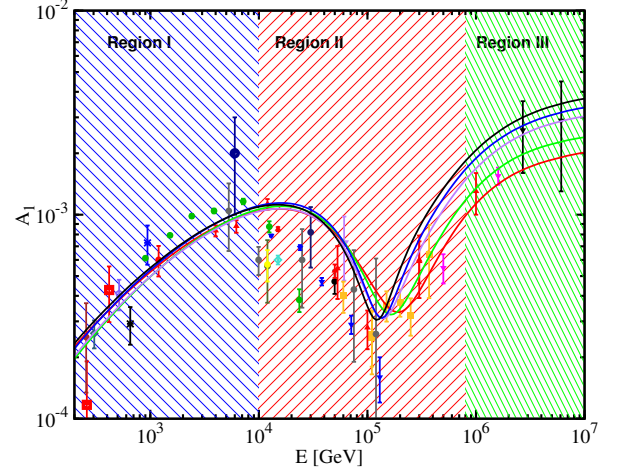


Fig. 6. Energy dependence of amplitudes of dipole anisotropy when adding all major CR elements together. Observational data are taken from [8] and references therein. See Fig. 3 for legends of lines.

of the local source under various  $Z_{\text{IH}}$  scenarios in order to fit the data well. The all-particle CR energy spectrum predicted from the SDP model is exhibited in Fig. 5, along with that from the Horandel spectrum, which is extracted from copious amounts of experimental data.

### C. Anisotropy and Solar Offset

It is proposed in the literature that the energy-dependent anisotropy and softening features in the energy spectra might have a common origin [33]. Figure 6 demonstrates that the energy-dependent CR anisotropy

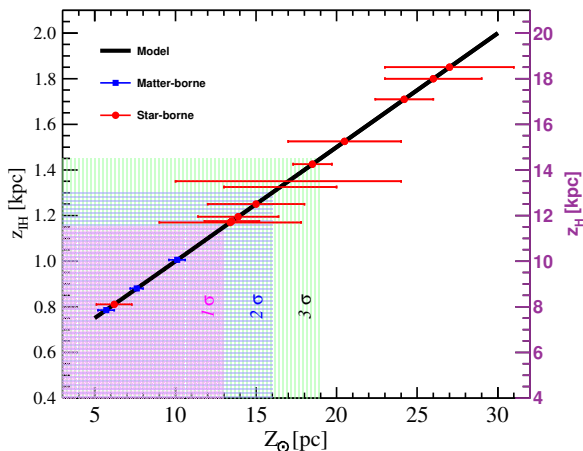


Fig. 7. The black solid line represents the relationship between displacement of the Sun from the (galactic plane) point ( $R_0, Z_0$ ) and the thickness of the halo. The right-hand axis also shows the total thickness of the halo taking  $\xi = 0.1$ . The three shaded areas are intervals corresponding to the goodness of model fit to PeV anisotropy at  $1\sigma$ ,  $2\sigma$ , and  $3\sigma$ . The blue rectangles and red bullets are solar displacement estimated with matter- and star-borne methods, respectively.

amplitudes can be well reproduced in this model. Considering the contribution of the local source, the anisotropy of all components can be divided into three regions by energies. In the lowest-energy region (region I), the anisotropy is influenced by the propagation coefficient and local sources, and the former dominates although the latter becomes important as the energy increases. The contribution of the local source to the anisotropy reaches its maximum value at tens of TeV and then decreases, and thus it is essential for the reproduction of the dip features in region II. At the highest-energy range (region III), the thicker the halo, the larger the anisotropy. In this region, the effect of the local source becomes limited and the propagation effect dominates. In region III, the model-calculated amplitudes vary. The goodness of model fit to the four observational points above PeV energy are 0.81, 0.43, 4.84, 10.16, and 16.92 for  $Z_{IH}$  adopted as 0.75, 1.0, 1.15, 1.3, and 1.45 kpc, respectively, and the p value of the latter three correspond to  $1\sigma$ ,  $2\sigma$ ,  $3\sigma$ , respectively. From this it can be seen that the inner halo is thicker than the typical value of a few hundred pc [43].

In addition, it is found that the PeV anisotropy is a good approach by which to constrain the halo thickness and also the solar offset, owing to the limited contribution of the nearby source in this energy range. It is known that the dipole anisotropy estimation is proportional to  $D_{xx}$  [24], the ratio of the parameterized diffusion coefficient and halo thickness, i.e.,  $D_{xx}/Z_H$ , is fixed by the observation of the ratio of B/C; therefore, the thickness of halo dominates the anisotropy. Specifically, the anisotropy is proportional to  $D_{xx}$ , and, in addition, to  $Z_H$  and the solar offset. On account of the little effect of the OH region,

the IH region has an effect on the anisotropy. To obtain the dipole anisotropy structure, the thickness of the halo increases linearly with the solar offset as shown as in Fig. 7. The three shaded regions are the goodness of model data fitted within  $1\sigma$ ,  $2\sigma$ , and  $3\sigma$ . If  $Z_{IH}$  is larger than 1.45 kpc, corresponding to the solar offset of 19 pc, the difference between the model-calculated and observed CR anisotropy measurements would be larger than  $3\sigma$ . This figure also shows the values of halo thickness with the solar displacement measured with matter- and star-borne methods in Fig. 1, under the relationship of halo thickness and solar offset estimated by PeV CR anisotropy.

#### IV. CONCLUSION

Measurements of CRs have entered a precise era thanks to the fast development of space-borne and ground-based experiments in recent years. Based on the new features of CR spectra, including the spectral hardening at  $\sim 200$  GV and softenings at  $\sim 10$  TV, together with the long-time enigma of the energy-dependent evolution of the dipole anisotropy features, an SDP framework with contributions from a local CR source was established and could explain most of these new observational facts [33].

In this work, the SDP model is extended to simultaneously study the CR spectra, anisotropy of CRs, and the Sun's offset from the galactic plane for, to the best of our knowledge, the first time. It is found that the primary CR protons and all-particle spectra, and the dip structure of the amplitudes of the total anisotropy, can be well reproduced after considering the Sun's offset. The thickness of the halo increases linearly with the displacement of the Sun, so a much thicker halo is required to counteract the affected anisotropy in the proposed model. Recent measurements, i.e., Fermi bubbles [40] and large-scale X-ray bubbles [37], support the point of a thick halo. Moreover, owing to the limited contribution of nearby sources, the dipole anisotropy in the PeV energy region can be used to estimate the value of  $D_{xx}$ , thus breaking the degeneracy of  $D_{xx}/Z_H$ , which is tuned by B/C ratio. Therefore, it is a good approach with which to constrain the halo thickness. However, with present observations of CR anisotropy, the proposed model shows that the solar offset prefers to be less than 19 pc. It is worth noting that this might be a new (model-dependent) method of constraining the solar displacement. It is expected that future precise measurements of the anisotropy in the energy range from  $\sim$  TeV to PeV by, e.g., LHAASO [14], could give a fine determination of the thickness of the halo, and, in addition, be used to test the proposed model and constrain the Sun's vertical location.

## ACKNOWLEDGMENTS

This work is supported by the National Key *R&D* Program of China (Grant No. 2018YFA0404202) and National Natural Science Foundation of China (Grant Nos. 11635011, 11875264, 11722328, 11851305, U1738205, and U2031110).

- 
- [1] Aartsen, M. G., Abbasi, R., Abdou, Y., et al. 2013, *ApJ*, 765, 55 1
  - [2] Abbasi, R., Abdou, Y., Abu-Zayyad, T., et al. 2012, *ApJ*, 746, 33 1
  - [3] Adriani, O., Barbarino, G. C., Bazilevskaya, G. A., et al. 2011, *Science*, 332, 69 1
  - [4] Aglietta, M., Alessandro, B., Antonioli, P., et al. 1996, *ApJ*, 470, 501 1
  - [5] Aguilar, M., Aisa, D., Alpat, B., et al. 2015, *Phys. Rev. Lett.*, 114, 171103 4
  - [6] Aguilar, M., Ali Cavasonza, L., Alpat, B., et al. 2017, *Phys. Rev. Lett.*, 119, 251101 4
  - [7] Ahlers, M. 2016, *Physical Review Letters*, 117, 151103 1
  - [8] Ahlers, M., & Mertsch, P. 2017, *Progress in Particle and Nuclear Physics*, 94, 184 4
  - [9] Ahn, H. S., Allison, P., Bagliesi, M. G., et al. 2010, *ApJ*, 714, L89 1, 4
  - [10] Amenomori, M., Bi, X. J., Chen, D., et al. 2017, *ApJ*, 836, 153 1
  - [11] An, Q., Asfandiyarov, R., Azzarello, P., et al. 2019, *Science Advances*, 5, eaax3793 1
  - [12] Antoni, T., Apel, W. D., Badea, A. F., et al. 2005, *Astroparticle Physics*, 24, 1 4
  - [13] Atkin, E., Bulatov, V., Dorokhov, V., et al. 2018, *Soviet Journal of Experimental and Theoretical Physics Letters*, 108, 5 1
  - [14] Bai, X., Bi, B. Y., Bi, X. J., et al. 2019, *arXiv e-prints*, arXiv:1905.02773 5
  - [15] Bartoli, B., Bernardini, P., Bi, X. J., et al. 2013, *Phys. Rev. D*, 88, 082001 1
  - [16] —. 2015, *ApJ*, 809, 90 1
  - [17] Bell, A. R. 1978, *MNRAS*, 182, 443 2
  - [18] —. 1978, *MNRAS*, 182, 147 2
  - [19] Biermann, P. L., Becker, J. K., Dreyer, J., et al. 2010, *ApJ*, 725, 184 1
  - [20] Blandford, R. D., & Ostriker, J. P. 1978, *ApJ*, 221, L29 2
  - [21] Bobylev, V. V., & Bajkova, A. T. 2016, *Astronomy Letters*, 42, 182 2, 3
  - [22] Case, G., & Bhattacharya, D. 1996, *A&AS*, 120, 437 2
  - [23] Evoli, C., Gaggero, D., Grasso, D., & Maccione, L. 2008, *J. Cosmology Astropart. Phys.*, 10, 018 2
  - [24] —. 2012, *Phys. Rev. Lett.*, 108, 211102 5
  - [25] Gaggero, D., Grasso, D., Marinelli, A., Urbano, A., & Valli, M. 2015, *ApJ*, 815, L25 1
  - [26] Garcia-Munoz, M., Mason, G. M., & Simpson, J. A. 1977, *ApJ*, 217, 859 2
  - [27] Giesen, G., Boudaud, M., Génolini, Y., et al. 2015, *J. Cosmology Astropart. Phys.*, 9, 23 1
  - [28] Guo, Y.-Q., & Yuan, Q. 2018, *Phys. Rev. D*, 97, 063008 2
  - [29] Hörandel, J. R. 2003, *Astroparticle Physics*, 19, 193 4
  - [30] Jin, C., Guo, Y.-Q., & Hu, H.-B. 2016, *Chinese Physics C*, 40, 015101 1
  - [31] Joshi, Y. C. 2007, *MNRAS*, 378, 768 2
  - [32] Liu, W., Bi, X.-J., Lin, S.-J., Wang, B.-B., & Yin, P.-F. 2017, *Phys. Rev. D*, 96, 023006 1
  - [33] Liu, W., Guo, Y.-Q., & Yuan, Q. 2019, *J. Cosmology Astropart. Phys.*, 2019, 010 1, 4, 5
  - [34] Liu, W., Yao, Y.-h., & Guo, Y.-Q. 2018, *ApJ*, 869, 176 2
  - [35] Mertsch, P., & Funk, S. 2015, *Phys. Rev. Lett.*, 114, 021101 1
  - [36] Panov, A. D., Adams, J. H., Ahn, H. S., et al. 2006, *arXiv e-prints*, astro 1
  - [37] Predehl, P., Sunyaev, R. A., Becker, W., et al. 2020, *Nature*, 588, 227 5
  - [38] Savchenko, V., Kachelrieß, M., & Semikoz, D. V. 2015, *ApJ*, 809, L23 1
  - [39] Schwadron, N. A., Adams, F. C., Christian, E. R., et al. 2014, *Science*, 343, 988 1
  - [40] Su, M., Slatyer, T. R., & Finkbeiner, D. P. 2010, *ApJ*, 724, 1044 5
  - [41] Thoudam, S., & Hörandel, J. R. 2012, *MNRAS*, 421, 1209 1
  - [42] —. 2014, *A&A*, 567, A33 1
  - [43] Tomassetti, N. 2012, *ApJ*, 752, L13 1, 2, 5
  - [44] Yao, J. M., Manchester, R. N., & Wang, N. 2017, *MNRAS*, 468, 3289 2, 3
  - [45] Yoon, Y. S., Anderson, T., Barrau, A., et al. 2017, *ApJ*, 839, 5 1
  - [46] Yuan, Q., Zhang, B., & Bi, X.-J. 2011, *Phys. Rev. D*, 84, 043002 1
  - [47] Zatsepin, V. I., & Sokolskaya, N. V. 2006, *A&A*, 458, 1 1